

# Electron acceleration by an intense laser pulse inside a density profile induced by non-linear pulse evolution

## Original Study

**Cite this article:** Pishdast M, Yazdanpanah J, Ghasemi SA (2018). Electron acceleration by an intense laser pulse inside a density profile induced by non-linear pulse evolution. *Laser and Particle Beams* **36**, 41–48. <https://doi.org/10.1017/S0263034617000970>

Received: 14 October 2017  
Accepted: 10 December 2017

**Key words:**  
Density profile; electron acceleration;  
non-linear pulse evolutions

**Author for correspondence:** Seyed Abolfazl Ghasemi, Plasma and Nuclear Fusion Research School, Nuclear Science and Technology Research Institute, Tehran, Iran.  
E-mail: [abo.ghasemi@gmail.com](mailto:abo.ghasemi@gmail.com)

M. Pishdast, J. Yazdanpanah and S. A. Ghasemi

Plasma and Nuclear Fusion Research School, Nuclear Science and Technology Research Institute, Tehran, Iran

### Abstract

By sophisticated application of particle-in-cell simulations, we demonstrate the ultimate role of non-linear pulse evolutions in accelerating electrons during the entrance of an intense laser pulse into a preformed density profile. As a key point in our discussions, the non-linear pulse evolutions are found to be very fast even at very low plasma densities, provided that the pulse length exceeds the local plasma wavelength. Therefore, these evolutions are sufficiently developed during the propagation of typical short density scale lengths occurred at high contrast ratios of the pulse, and lead to plasma heating via stochastic acceleration in multi-waves. Further analysis of simulation data at different physical parameters indicates that the rate of evolutions increases with the plasma density leading to higher plasma heating and overgrown energetic electrons. In the same way, shortening the density scale length results into increase in the evolution rate and, simultaneously, decrease in the interaction time. This behavior can describe the observed optimum value of pre-plasma scale length for the maximum electron heating.

### Introduction

The intrinsic, long pedestal of an intense short laser pulse unavoidably leads to the production of plasma coronas (pre-plasma) with finite scale-lengths in the target front, having profiles with densities below the critical value. At typical contrast ratios now available, pre-plasmas with density scale lengths of a few to tens of microns are usually produced as described in (Paradkar *et al.*, 2011), which may significantly influence the interaction in several ways. Especially, it may affect the particle acceleration, a subject which has attracted a vast number of attention, due to its potential applications. It has been frequently observed that a strong correlation exists between the density scale length and the observed spectrum of the accelerated particles (Paradkar *et al.*, 2011). For example, much recently, one-dimensional (1D) particle-in-cell (PIC) simulation of  $10^{19}$ – $10^{21}$  W/cm<sup>2</sup> intensity laser interaction with solid target for different preformed plasma scale lengths (1–15  $\mu$ m) reveal an increase in mean and maximum energy of fast electrons with an increase in the plasma scale length (Paradkar *et al.*, 2011). However, despite many extensive studies by Paradkar *et al.* (2011); Santala *et al.* (2000), Mackinnon *et al.* (2001), Yabuuchi *et al.* (2010), Culfa *et al.* (2014), Culfa *et al.* (2017), Culfa *et al.* (2016), Andreev *et al.* (2016), Fang *et al.* (2016), and Holkundkar and Gupta (2008), the exact mechanism of impact of pre-plasma in a particle acceleration has remained still unclear.

An important question regarding the interaction of a laser pulse with pre-plasma, which is an underdense plasma, is the origin of super-hot electrons typically observed in experiments and simulations. A well-understood acceleration mechanism, which is active in the underdense plasma is parametric amplification in the ion channel, proposed by Pukhov *et al.* (1999). However, this mechanism is essentially multi-dimensional and is realized inside the preformed plasma channels or in the so-called self-focusing regime, both of which rely on relatively long propagation distances in long plasma profiles. This is while the typical scale lengths observed in actual pre-plasmas are of the order of few tens of microns and may not support the mentioned acceleration mechanisms.

Therefore, quickly operating mechanisms with being 1D in nature are very important in relation to pre-plasmas. Numbers of generically 1D mechanisms have been suggested by authors, including non-linear wave break in the vacuum–plasma interface published by Chakhmachi *et al.* (2017) and Bulanov *et al.* (1998), non-wakefield interaction by Robinson *et al.* (2013), and stochastic heating by Paradkar *et al.* (2011), Sheng *et al.* (2004), and Boudier *et al.* (2007). According to recent studies, Paradkar *et al.* (2011), Sheng *et al.* (2004), and Wu *et al.* (2017), the last one is predominant in the case of pre-plasma.

The stochastic heating is based on the fundamental phenomenon of chaotic electron motion within the counter-propagating plane electromagnetic (EM) waves, which may lead

to net energy gain by the electron, despite the situation with a single plane wave (Mendoca, 1983). Interestingly, the operation of the mechanism does not require that both interacting waves achieve very high amplitudes, but rather, coexistence of a weak counter-propagating wave suffices along with an intense main pulse, that is, the auxiliary wave may have an amplitude of a few percent of the main pulse (Sheng *et al.*, 2004; Mendoca, 1983). This means that, this mechanism can be easily realized in an underdense plasma, as the plasma is proven to many scattering instabilities as mentioned by Paradkar *et al.* (2011), Sheng *et al.* (2004), and Wu *et al.* (2017), provided that the instabilities be quickly established.

Regarding realization of the stochastic heating in actual plasmas, a key question is the development of the scattered radiation up to the threshold for plasma heating by chaotic motion in terms to Mendoca (1983). Also, given the plasma density variations during the laser entrance from the plasma boundary, it is very important to understand the contribution of wave break in the vacuum–plasma interface discussed in [Chakhmachi *et al.*, 2017; Bulanov *et al.*, 1998], which comes in conjunction with stochastic heating. Both these topics have remained still far from being completely understood in the context of existing studies. In this regard, as the light is eventually reflected from the critical surface, the plasma heating may loosely be attributed to the stochastic motion in the counter-propagating waves from the reflection. This is while we have found that, even in the absence of laser pulse backscattering from critical density or effect, there is a radiation scattering at the early stage of interaction which is responsible for plasma heating and electron acceleration. However, as the plasma scattering at high intensities and short pulse lengths are highly anomalous, (Tzeng *et al.*, 1996), the accurate quantitative examination of the establishment of plasma scatterings does not completely rely on the present theoretical models and usually needs numerical simulations.

In this paper, via sophisticated application of the PIC method, we numerically investigate the evolutions of radiation scattering and describe their relation to electron accelerations. In this regard, it is worthwhile to mention that Paradkar *et al.* (2011) demonstrate the ultimate role of pulse evolutions in particle acceleration, but the nature of pulse scatterings remained unexplored. As a key point, we clearly demonstrate the quick establishment of anomalous plasma scattering and describe the phenomenon in detail. We also find that the nature of scatterings is not essentially affected by the profile shape. Further, it is found that scattered waves support the stochastic heating descriptions in initially low-temperature plasma ( $k_B T_e \sim 10^{-4} m_e c^2$ ) in the absence of wave break in the vacuum–plasma interface as a possible pre-heating mechanism. In fact, the wave break turns marginal when the pulse length exceeds the plasma wavelength.

The paper is organized into different sections as follow. A brief description of our PIC modeling is mentioned in the section “PIC simulation characteristics” and simulation results, discussion, and conclusion are presented in the section “Results and discussion”.

### PIC simulation characteristics

The 1D 3 V PIC code equipped with Fourier analysis, developed by Yazdanpanah and Anvary (2012, 2014), has been used in our simulations. In addition to PIC solution, this code is able to give the quasi-static fluid solution simultaneously.

Here we simulate the interaction of P-polarized laser pulses of  $1 \mu\text{m}$  wavelength with intensities denoted by dimensionless

amplitudes  $a_0 = eE_0/(m_e \omega c) = 1, 2$ , propagating in the  $+x$ -direction with hydrogen-like plasmas having different plasma profiles.  $a_0$  is the normalized transverse vector potential maximum amplitude, which relates to the laser intensity  $I$  as  $I = 1.37 \times 10^{18} [a_0/\lambda (\mu\text{m})]^2 (\text{W}/\text{cm}^2)$ . A long semi-sinusoidal laser pulse with 300 fs temporal duration has been considered in the simulations. The laser rises up within a first half of the pulse duration and then falls down to zero in the second half. A spatial resolution of 5 nm (200 cells per wavelength) with 64 particles per cell is used in the simulations. The considered cell size ensures no numerical heating and well resolved of the lowest scale length. The absorbing boundary condition is considered for particles and laser beam. The initial plasma temperature is set to be  $k_B T_{e0}/m_e c^2 = 10^{-4}$  (50 eV) and the ions supposed to be cold and immobile.

The simulations have been performed in two different electrostatic (ES) and EM modes. In the ES mode, the transverse plasma current through Maxwell equations is ignored to eliminate the pulse evolutions because of scattering and modulation. Using this trick, the plasma optical response is artificially eliminated and the laser propagates unaffected through the plasma and so the radiation scattering effects on plasma heating are neglected. The equation of motion and the Poisson’s equation are treated as in the usual EM model.

In order to outline the basic physics, in addition to variable plasma profiles, we firstly consider three different step-like density profiles at three density values,  $0.01n_c$ ,  $0.03n_c$ , and  $0.05n_c$ , where  $n_c$  is the plasma critical density. In all these simulations, the pulse length satisfies  $L_p > \lambda_p = c/\omega_p$  (long pulse), meaning the pulse may undergo scatterings and modulations. Afterward, we go through the investigation of pre-plasma effects by using exponential and linear plasma density profiles having different initial scale lengths ranging from 2 to  $80 \mu\text{m}$ , to find out the optimum value of pre-plasma scale length for electrons acceleration.

The initial pre-plasma densities for linear profile were chosen in such a way that it rises with constant ramp until reaches to  $2n_c$  at  $2L_p$  and then remains at this constant density for  $10 \mu\text{m}$  (Figure 1), where  $L_p$  denotes the pre-plasma density scale length. The exponential profile, on the other hand, is considered as  $n_e = n_{e0} e^{-(x_0 - x)/L_p}$ , where  $n_{e0} = 2n_c$  and  $x_0$  is the starting point of density’s flat top. For all the scale lengths, the time-integrated electrons energy spectrum are calculated at the end of the flat top part of the density within  $1 \mu\text{m}$  space to ensure that relativistic critical density ( $\gamma_{\text{OSC}} n_c$ ) would prevent laser pulse penetration to that point and at the time that it gets saturated. Here,  $\gamma_{\text{OSC}}$  is defined for the laser dimensionless amplitude as  $\gamma_{\text{OSC}} = \sqrt{1 + a_0^2/2}$ . Meanwhile, various simulation boxes are

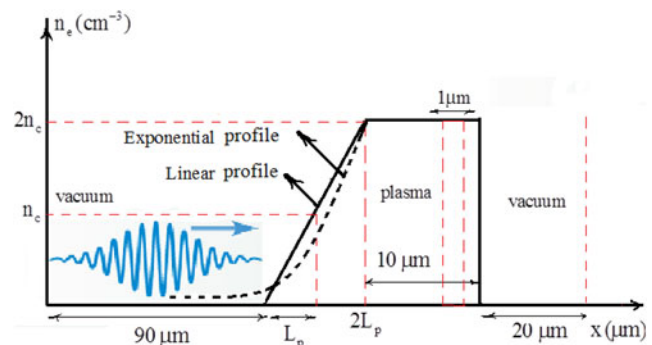


Fig. 1. Schematic representation of the simulation setup.

considered depending on the values of scale lengths. But in all simulations 90 and 20  $\mu\text{m}$  vacuum gaps are applied to the first and last parts of the box, respectively (Figure 1).

## Results and discussion

As predicted by the linear theory, the plasma strongly reacts against the EM field oscillations and produces the scattered fields such as Raman forward scattering (RFS) and Raman backward scattering (RBS) (Kruer, 1988). RBS is the fastest growing of Raman scattering instabilities and its e-folding time can be as short as  $1/\omega_0$  in the strong coupling regime (Stabrook & Kruer, 1983; Stabrook *et al.*, 1980). On the other hand, for RFS (Decker *et al.* 1996; Mori and Decker, 1994), which is essentially active at densities below the quarter of the critical density  $n_{e0} < 0.25n_c$ , the e-folding time is of the order of  $n_c/n_{e0}\omega_0$ ; therefore, it happens at the later time of the laser–plasma interaction.

As in the RFS, the excited plasma wave (Langmuir) has a phase-space velocity close to the speed of light and it is able only to accelerate electrons with initial high velocities. Such acceleration is realized for example when a long, intense laser pulse drives a very high amplitude plasma wave at the ultimate stages of modulation via RFS in the so-called self-modulated laser Wakefield acceleration (SMLWFA) published by Esarey *et al.* (2009). Another example of RFS acceleration is an acceleration of possibly pre-heated electrons via other active mechanisms. However, both of these scenarios are a part of long-term system behaviors and may not happen in the initial stages of interaction and short density profiles. Despite this character of RFS action, RBS-excited plasma wave has the phase velocity  $v_p/c < 1$ , so that this type of plasma wave can trap the background thermal electrons described in (Esarey *et al.*, 2009), as soon as the RBS mode grows to high amplitudes. Therefore, in a short density scale length, the electrons are most likely preheated firstly by Raman backward radiation, and then are subjected to acceleration in counter-propagating waves of incident pump mode and reflected mode from the critical layer (Paradkar *et al.*, 2011), and the acceleration in both stages is of stochastic type which is essentially EM in nature.

On the other hand, space-charge oscillations which are generally excited in interactions of intense finite laser pulses are subjected to non-linear wave break (Whitham, 1974) in the vacuum–plasma interface (Bulanov *et al.*, 1998). This wave break, which is ES in nature published by Chakhmachi *et al.* (2017), can accelerate electrons and may be considered as a generic mechanism being active at the front of the target and competing with RBS. In our simulations, we are able to isolate the wave-brake effect via choosing the ES mode and clarify its sole effect. Additionally, we are able to give a detailed account of all above-mentioned phenomena in the fully non-linear regime.

Figure 2 shows the intensity spectrum of total radiation (laser pulse plus scattered fields) versus wavenumber at different interaction times, when a 300 fs duration laser pulse strikes a step-like plasma density at  $0.01n_c$ . The results of both ES and EM modes are depicted in this figure. It is obvious from the blue diagram (covered by yellow), which shows the radiation spectrum of the incident laser before the interaction, that the laser is a single-mode pulse at  $k = k_0$ . The yellow diagram is related to the radiation spectrum for the ES mode at 0.3 ps after the interaction. This diagram indicates that, as it was expected, no pulse evolution occurs during interaction in this mode. Other diagrams show the total radiation spectrum at 0.1, 0.3, 1.8, and 2.7 ps after

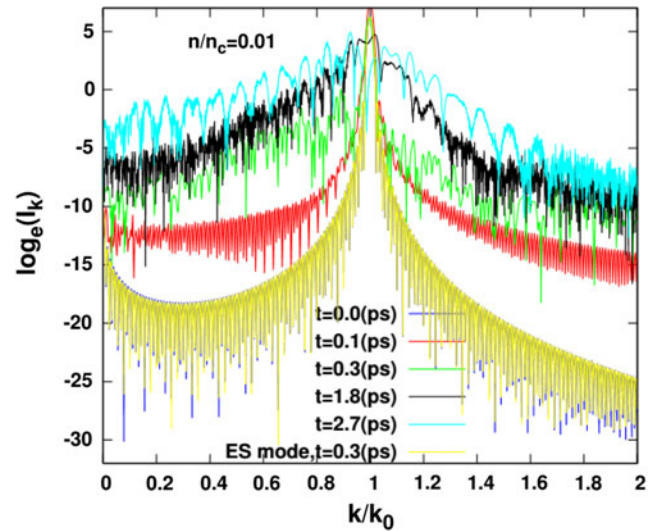


Fig. 2. The intensity spectrum of total radiation against wavenumber at different interaction times for  $a_0 = 2$ .

interaction for the EM mode. It is found that the pulse-scattering mechanism starts at the initial stage of interaction and then as the time passes, scattering mechanism could be attributed to Raman scattering, which begins at the very beginning and continuously develops up to long times. Generally, in the positive wavenumber space considered here, the RBS modes appear on both sides of the central mode.

Figures 3a–3d show PIC and fluid simulation results of the plasma longitudinal electric field and transverse vector potential of the laser pulse ( $a_y$ ) at 0.1, 0.3, and 2.7 ps after interaction for EM, Figures 3a–3c and ES, Figure 3d modes respectively for  $n = 0.01n_c$ . A noticeable mismatch is observed between PIC results in the EM mode and fluid solutions at initial stages (see Figs 3a and 3b). This while, according to Figure 3c, at long times, the results of PIC and fluid simulations at beginning and vicinity of the pulse turn close to each other which implies the relative stability of the scatterings. This behavior corresponds to the self-modulation of laser pulse due to RFS. The behavior of the ES mode is shown in Figure 3d. As it was expected, no pulse scattering and modulation occur in this case. Figures 3e–3h show the longitudinal momentum diagram related to Figures 3a–3d. Figures 3e–3g, which are obtained in the EM mode, show the initiation of plasma heating at the very beginning and its continuation as the time passes, indicating more plasma heating with an increment of scatterings results. On the other hand, as Figure 3h indicates, there is no plasma heating at 0.3 ps for the ES mode that rules out the efficient effectiveness of wave brake in the plasma–vacuum interface.

To understand the importance of the initial density value of mentioned electron acceleration, we perform EM simulations of step plasma profiles at different initial plasma densities. Figures 4a–4d, represent the radiation spectrum for  $0.01n_c$ ,  $0.03n_c$ , and  $0.05n_c$  initial densities at different interaction times 0.1, 0.3, and 0.8 and 2.7 ps. Results show that increasing the initial plasma density leads to faster growth of scatterings. So, it is expected that the increase of the scatterings with plasma density, results in more effective plasma heating and electron acceleration at higher initial plasma densities. This expectation is confirmed in the PIC and fluid simulation results of the plasma longitudinal electric field,

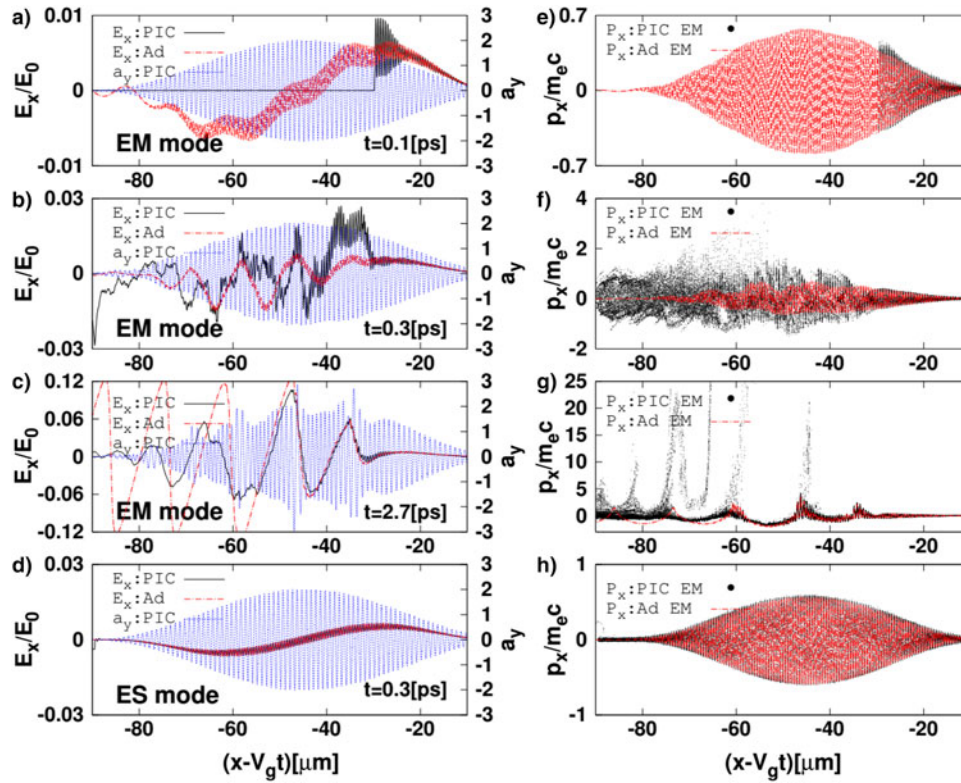


Fig. 3. PIC and fluid simulation results of the (a–d) plasma longitudinal wave and the laser pulse amplitude, and (e–h) electron phase-space diagram at 0.1–2.7 ps after interaction for the EM and ES modes,  $n/n_c=0.01$  and  $\sigma_0=2$ .

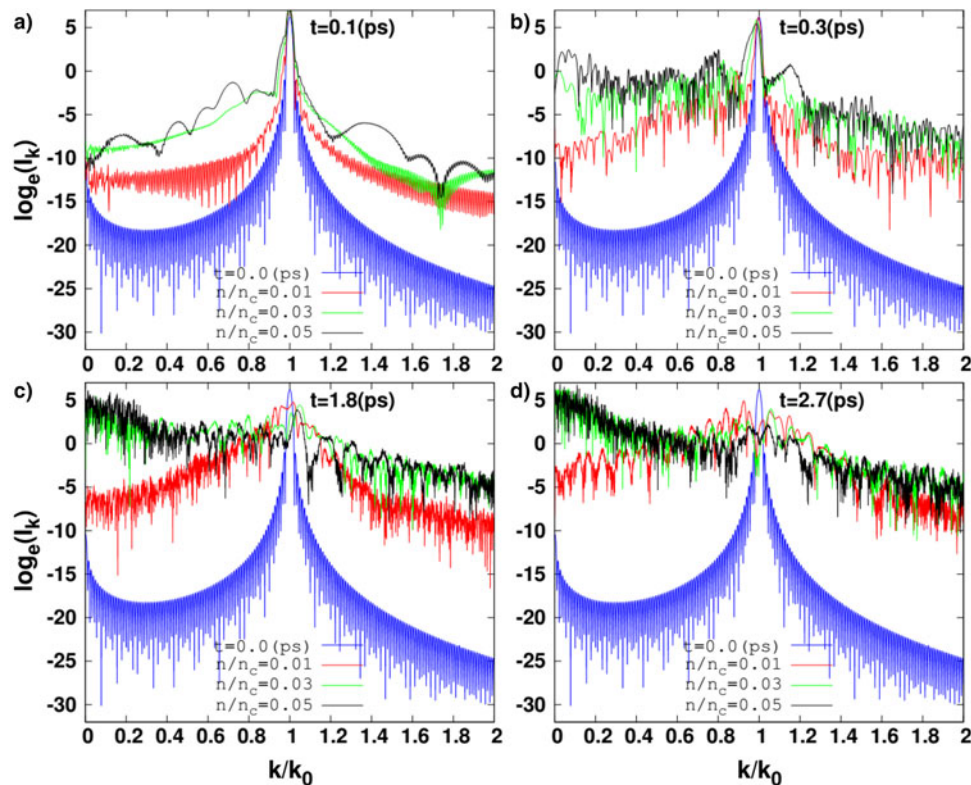
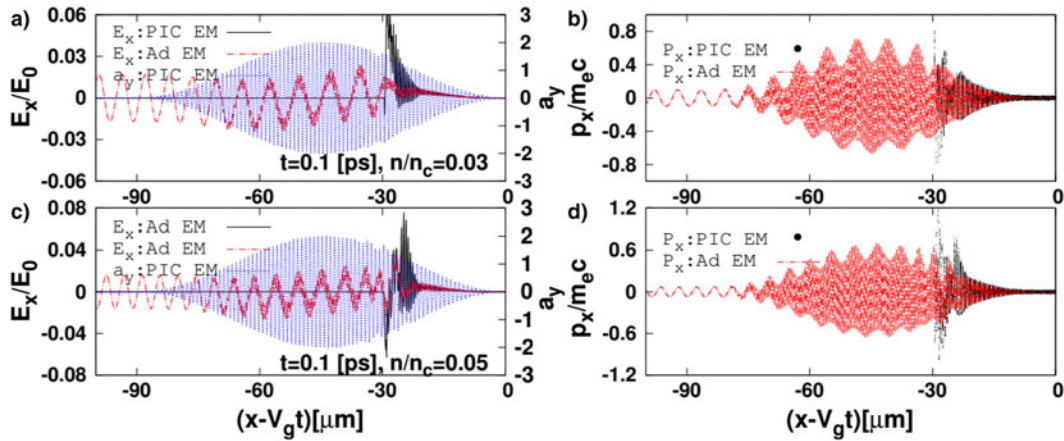


Fig. 4. The radiation intensity against wavenumber at  $0.01n_c$ ,  $0.03n_c$ ,  $0.05n_c$  plasma initial densities at different times of interaction 0.1–2.7 ps for  $\sigma_0=2$ .



**Fig. 5.** PIC and fluid simulation results of the (a, b) plasma longitudinal wave and the laser pulse transverse vector potential and (c, d) electron longitudinal momentum diagram at 0.1 ps for  $n/n_c = 0.03$  and  $0.05$  for  $a_0 = 2$ .

transverse vector potential and electron longitudinal momentum diagram depicted in Figures 5a–5d at 0.1 ps, respectively for  $0.03n_c$  and  $0.05n_c$ .

In terms to Figure 5, it is understood that, there is more powerful longitudinal electric wakefield and also more plasma heating for higher initial plasma densities even at 0.1 ps after interaction which according to Figure 4, is as a result of higher scattering for higher densities. These behaviors become clearer at later times of interaction, which typically are shown in Figure 6 for 0.3 ps.

The results outlined so far indicate that during the laser interaction with an underdense plasma in 1D geometry, a generic acceleration mechanism is quickly stabilized via non-linear pulse evolutions which are of EM type. For long pulse length considered here, the density transition (variation) in the vacuum-plasma interface does not play an efficient role as the wave

break does not really occur even at sharp density transition. Therefore, the generic physics of acceleration in pre-plasma with arbitrary profile shape does not alter dramatically with respect to the step density. In fact, a variable plasma profile may be considered as a definite assembly of large numbers of thin step profiles at different densities ranging between the extreme values of the variable profile. To better understand the behaviors of variable profiles, we study density profiles with a wide range of scale lengths,  $L_p$ , from 2 to  $80 \mu\text{m}$ , and with both linear and exponential shapes. The linear density profile is observed in experiments with gas targets (Willingale *et al.*, 2006), and used in simulation studies for example by Lefebvre and Bonnaud (1997). The exponential profile, on the other hand, is typically considered in experiments with solid targets (Santala *et al.*, 2000; Ovchinnikov *et al.*, 2013; Culfa *et al.*, 2016).

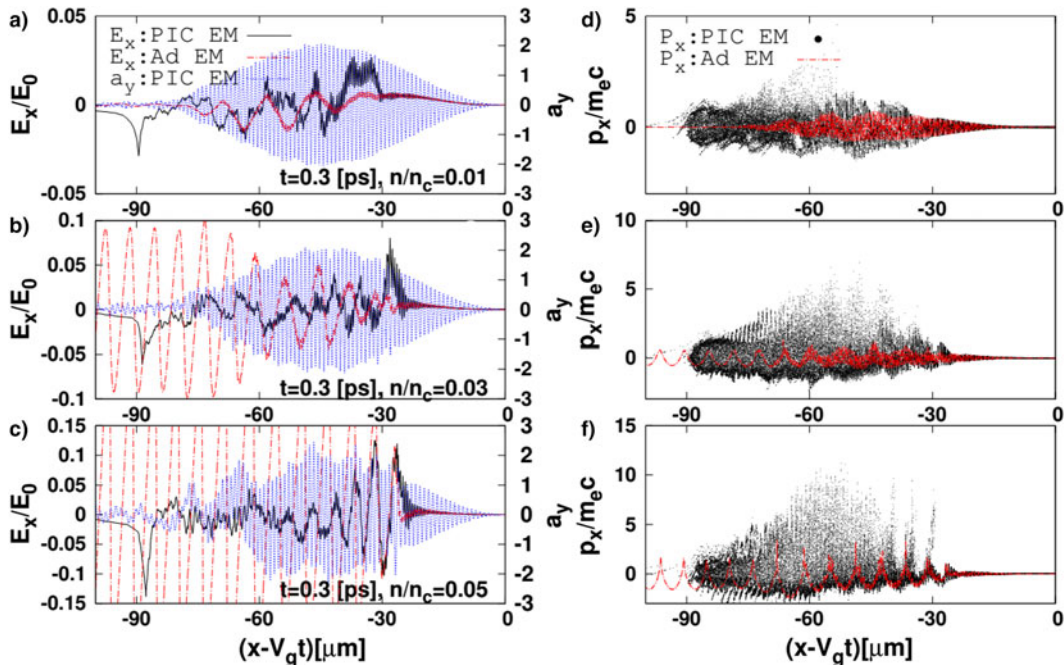


**Fig. 6.** PIC and fluid simulation results of the (a–c) plasma longitudinal wave and the laser pulse transverse vector potential and (d–f) electron longitudinal momentum diagram at 0.3 ps for  $n/n_c = 0.01, 0.03,$  and  $0.05$  for  $a_0 = 2$ .

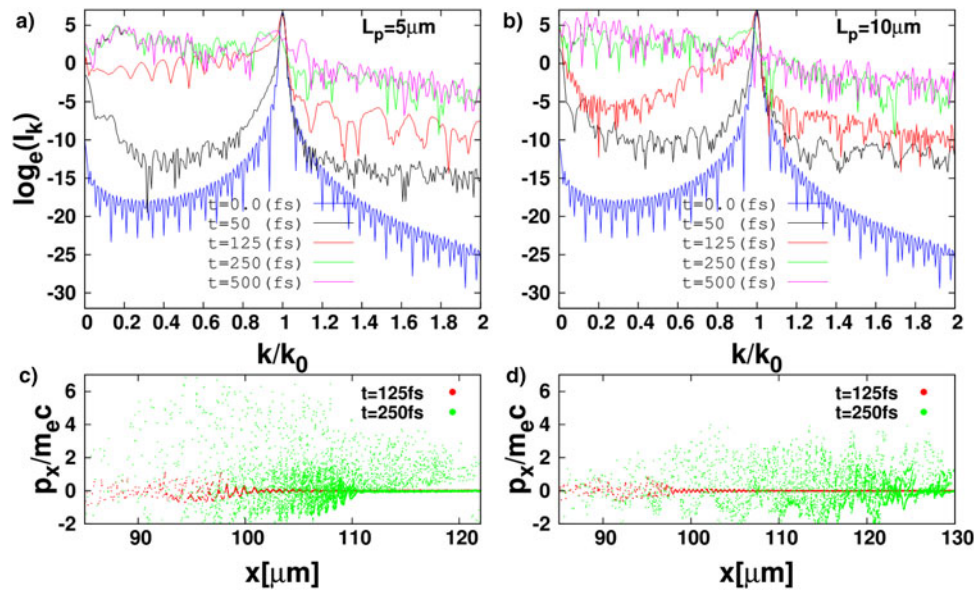


Fig. 7. (a, b) The radiation intensity and (c, d) phase-space diagram for two different, 5 and 10  $\mu\text{m}$  exponential scale lengths at different times for  $\sigma_0 = 1$ .

Evolution of the radiation spectrum, and an instance of longitudinal phase space for two different scale lengths,  $L_p = 5$  and 10  $\mu\text{m}$ , have been depicted in Figures 7 and 8 for exponential and linear profiles, respectively. Figures 7, 8a, and 8b show that there are scattering at the very beginning of the interaction time for both 5 and 10  $\mu\text{m}$  scale lengths. Comparing these figures implies that at the initial stages of interaction, there is a faster-growing scattering for shorter scale lengths which is in agreement with our mentioned results in the case of step density, as the scattering rate increases at higher densities. Self-consistent evolutions of phase space are presented in Figures 7, 8c, and 8d, showing the plasma heating at very short onset time of interaction.

According to Figures 7c and 7d, in the case of an exponential profile, higher electron heating occurs for shorter scale length (5  $\mu\text{m}$ ). This is while, in the case of a linear profile, it can be

seen in Figures 8c and 8d that larger scale length (10  $\mu\text{m}$ ) leads to higher electron heating.

In order to study the ultimate effect of variations of scattering rate and electron heating versus the scale length, we consider the electrons energy distribution function together with time history of hot electrons mean energy for different scale lengths (2–80  $\mu\text{m}$ ), for both exponential and linear profiles, as plotted in Figures 9a–9d. It is clearly observed that electrons have the highest maximum and mean energies at a median scale length, which is 5  $\mu\text{m}$  for exponential profile and 20  $\mu\text{m}$  for the linear profile, that is, an optimum scale length is expected. This behavior may be described in terms of results and behaviors obtained so far: It is reasonable to assume that the net energy gain by electrons is proportional to a factor of  $\propto \tau_{\text{int}} R$ , where  $R$  is the evolution rate of pulse and  $\tau_{\text{int}}$  is the interaction time. As observed above,

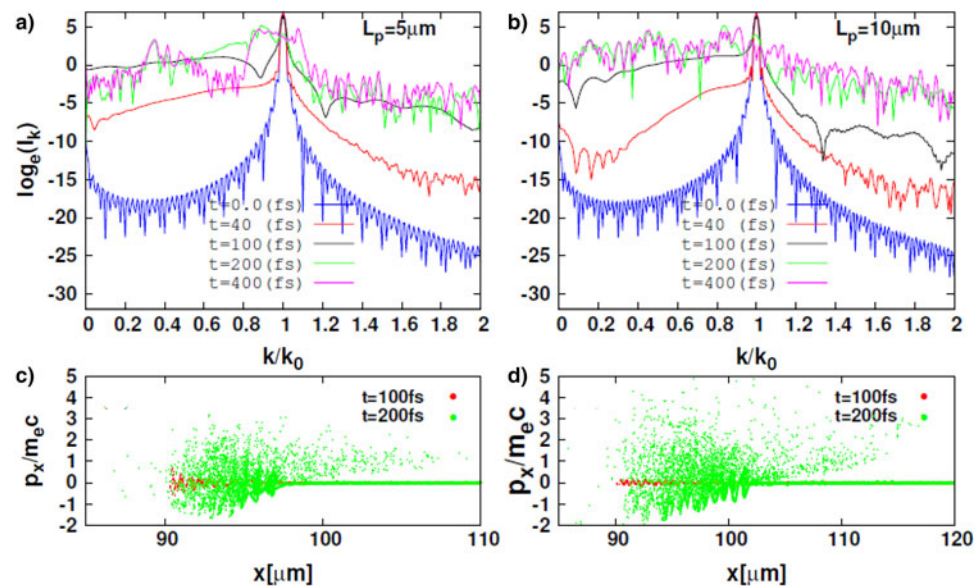
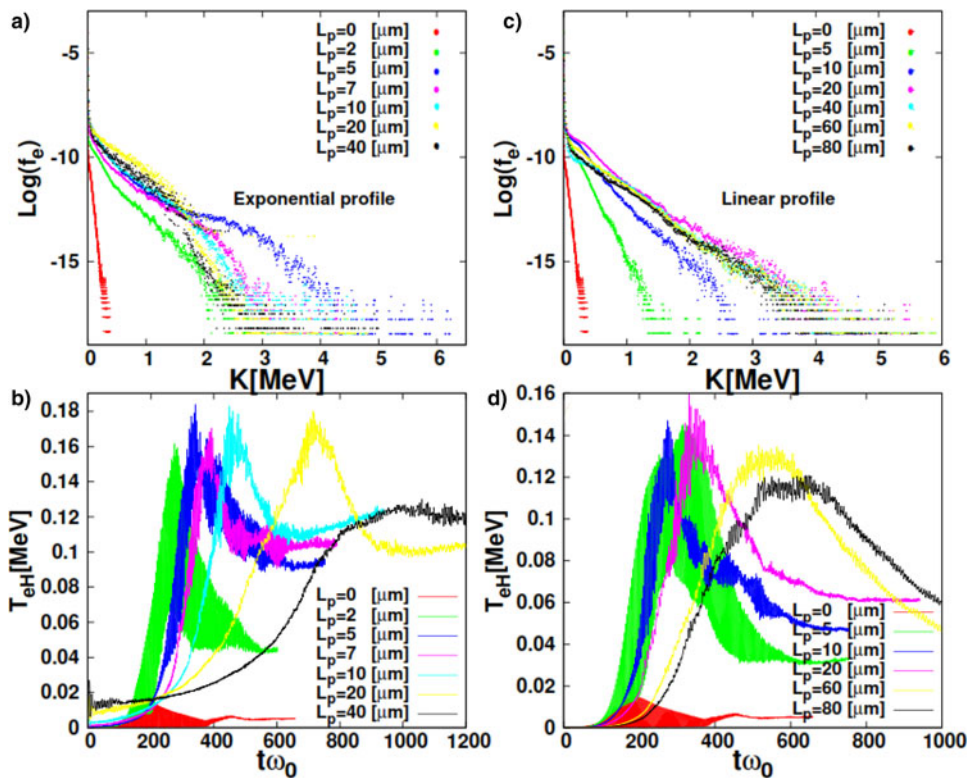


Fig. 8. (a, b) The radiation intensity and (c, d) phase-space diagram for two different, 5 and 10  $\mu\text{m}$  linear scale lengths at different times for  $\sigma_0 = 1$ .



**Fig. 9.** (a) Electrons energy distribution function, (b) hot electrons mean energy, for exponential scale lengths, and (c, d) for linear scale lengths at  $a_0 = 1$ .

shortening the density scale length results into increase in the evolution rate ( $R$ ) and, simultaneously, decrease in the interaction time ( $\tau_{int}$ ). As these effects compete with each other an optimum is expected.

In conclusion, we have demonstrated the ultimate role of non-linear pulse evolutions in accelerating electrons during the entrance of an intense laser pulse into a preformed density profile. As a key point in our discussions, the non-linear pulse evolutions have been found to be very fast even at very low plasma densities; therefore, they are sufficiently developed during the propagation of typical short density scale lengths occurred at high contrast ratios of the pulse, and lead to plasma heating via stochastic acceleration in multi-waves. Further, simulations data at different physical parameters have been presented and analyzed, and used to describe the observed optimum value of the pre-plasma scale length for the maximum electron heating.

## References

- Andreev NE, Pugachev LP, Povarenitsyn ME and Levashov PR (2016) Electron acceleration at grazing incidence of a sub picosecond intense laser pulse onto a plane solid target. *Laser and Particle Beams* **34**, 115–122.
- Boudier A, Patin D and Lefebvre E (2007) Stochastic heating in ultra high intensity laser-plasma interaction. *Laser and Particle Beams* **25**, 169.
- Bulanov SV, Naumova NM, Pegoraro F and Sakai J (1998) Particle injection into the wave acceleration phase due to nonlinear wake wave breaking. *Physical Review E* **58**, R5257.
- Chakhmachi A, Khalilzadeh E, Pishdast M and Yazdanpanah J (2017) Numerical study of the wave-break in the vacuum-plasma interface during the interaction of an intense laser pulse. *AIP Advances* **7**, 085317.
- Culfa O, Tallents GJ, Wagenaars E, Ridgers CP, Dance RJ, Rossal AK, Gray RJ, Mckenna P, Brown CDR, James SF, Hoarty DJ, Booth NA, Robinson PL, Lancaster KL, Pikuz SA, Faenov AY, Kampfer T, Schulze KS, Uschmann I and Woolsey NC (2014) Hot electron production

in laser solid interactions with a controlled pre-pulse. *Physics of Plasmas* **21**, 043106.

- Culfa O, Tallents GJ, Rossal AK, Wagenaars E, Ridgers CP, Murphy CD, Dance RJ, Gray RJ, Mckenna P, Brown CDRS, James F, Hoarty DJ, Booth N, Robinson APL, Lancaster KL, Pikuz SA, Faenov AY, Kampfer T, Schulze KS, Uschmann I and Woolsey NC (2016) Plasma scale-length effects on electron energy spectra in high-irradiance laser plasmas. *Physical Review E* **93**, 043201.
- Culfa O, Tallents GJ, Korkmaz ME, Rossal AK, Wagenaars E, Ridgers CP, Murphy CD, Booth N, Carroll DC, Wilson LA, Lancaster KL and Woolsey NC (2017) Plasma scale length effects on protons generated in ultra-intense laser-plasmas. *Laser and Particle Beams* **35**, 58–63.
- Decker CD, Mori WB, Katsouleas T and Hinkel DE (1996) Spatial temporal theory of Raman forward scattering. *Physics of Plasmas* **3**, 1360.
- Esarey EC, Schroeder B and Leemans WP (2009) Physics of laser-driven plasma-based electron accelerators. *Reviews in Modern Physics* **81**, 1229.
- Fang Y, Xulei G, Yang S, Wenqing W, Tongpu Y, Feng L, Chen M, Jingquan L, Xiaohui Y, Zhengming S and Zhang J (2016) Different effects of laser contrast on proton emission from normal large foils and transverse-size-reduced targets. *Plasma Physics and Controlled Fusion* **58**, 075010, 7 pp.
- Holkundkar A and Gupta NK (2008) Effect of initial plasma density on laser induced ion acceleration. *Physics of Plasmas* **15**, 123104.
- Kruer WL (1988) *The Physics of Laser Plasma Interactions*. Redwood City: Addison-Wesley.
- Lefebvre E and Bonnaud G (1997) Nonlinear electron heating in ultrahigh-intensity-laser-plasma interaction. *Physical Review E* **55**(1), 1011–1014.
- Mackinnon AJ, Borghesi M, Hatchett S, Key MH, Patel PK, Campbell H, Schiavi A, Snavely R, Wilks SC and Willi O (2001) Effect of plasma scale length on multi-MeV proton production by intense laser pulses. *Physical Review Letters* **86**(9), 1769(4).
- Mendoca JT (1983) Threshold for electron heating by two electromagnetic waves. *Physical Review A* **28**, 3592.
- Mori WB and Decker CD (1994) Raman forward scattering of short-pulse high intensity lasers. *Physical Review Letters* **72**(10), 1482(4).
- Ovchinnikov VM, Schumacher DW, McMahon M, Chowdhury EA, Chen CD, Morace A and Freeman RR (2013) Effects of pre-plasma

- scale length and laser intensity on the divergence of laser-generated hot electrons. *Physical Review Letters* **110**, 065007.
- Paradkar BS, Wei MS, Yabuuchi T, Steohen RB, Haines MG, Krasheninnikov SI and Beg FN** (2011) Numerical modeling of fast electron generation in the presence of preformed plasma in laser-matter interaction at relativistic intensities. *Physical Review E* **83**, 046401.
- Pukhov A, Sheng ZM and Meyer-Ter-vehn J** (1999) Particle acceleration in relativistic laser channels. *Physics of Plasmas* **6**, 2847.
- Robinson APL, Arefiev AV and Neely D** (2013) Generating super-ponderomotive electrons due to a non-wake-field Interaction between a laser pulse and a longitudinal electric field. *Physical Review Letters* **111**, 065002.
- Santala MIK, Zepf M, Watts I, Beg FN, Clark E, Tatarakis M, Krushelnick K and Dangor AE** (2000) Effect of the plasma density scale length on the direction of fast electrons in relativistic laser-solid interactions. *Physical Review Letters* **84**(7), 1459(4).
- Sheng ZM, Mima K, Zhang J and Meyer-Ter-vehn J** (2004) Efficient acceleration of electrons with counter-propagating intense laser pulses in vacuum and under-dense plasma. *Physical Review E* **69**, 016407.
- Stabrook K and Kruer WL** (1983) Theory and simulation of Raman backward and forward scattering. *Physics of Fluids* **26**(7), 1892–1903.
- Stabrook K, Kruer WL and Lasinski BF** (1980) Heating by Raman backscatter and forward scatter. *Physical Review Letters* **45**(17), 1399–1403.
- Tzeng KC, Mori WB and Decker CD** (1996) Anomalous absorption and scattering of short-pulse high-intensity lasers in under-dense plasmas. *Physical Review Letters* **76**, 3332.
- Whitham GB** (1974) *Linear and Nonlinear Waves*. New York: John Wiley and Sons.
- Willingale L, Mangles SPD, Nilson PM, Clarke RJ, Dangor AE, Kaluza MC, Karcch S, Lancaster KL, Mori WB, Najmudin Z, Schreiber J, Thomas AGR, Wei MS and Krushelnick K** (2006) Collimated multi-meV ion beams from high-intensity laser interactions with under-dense plasma. *Physical Review Letters* **96**, 245002.
- Wu D, Krasheninnikov SI, Luan SX and Yu W** (2017) Identifying the source of super-high energetic electrons in the presence of pre-plasma in laser-matter interaction at relativistic intensities. *Nuclear Fusion* **57**, 016007.
- Yabuuchi T, Paradkar BS, Wei MS, King JA, Beg FN, Stephens RB, Nakanii N, Hatakeyama M, Habara H, Mima K, Tanaka KA and Larensen JT** (2010) Transport study of intense-laser-produced fast electrons in solid targets with a pre-plasma created by a long pulse laser. *Physics of Plasmas* **17**, 060704.
- Yazdanpanah J and Anvary A** (2012) Time and space extended-particle in cell model for electromagnetic particle algorithms. *Physics of Plasmas* **19**, 03310.
- Yazdanpanah J and Anvary A** (2014) Effects of initially energetic electrons on relativistic laser-driven electron plasma waves. *Physics of Plasmas* **21**, 023101.